Comparison of Orthogonal Frequency-Division Multiplexing and Pulse-Amplitude Modulation in Indoor Optical Wireless Links

Daniel J. F. Barros, Sarah K. Wilson, *Senior Member, IEEE,* and Joseph M. Kahn, *Fellow, IEEE*

***Abstract*—We evaluate the performance of three direct-detection orthogonal frequency-division multiplexing (OFDM) schemes in combating multipath distortion in indoor optical wireless links, comparing them to unipolar M-ary pulse-amplitude modulation (*M*-PAM) with minimum mean-square error decision-feedback equalization (MMSE-DFE). The three OFDM techniques are DC-clipped OFDM and asymmetrically clipped optical OFDM (ACO-OFDM) and PAM-modulated discrete multitone (PAM-DMT). We describe an iterative procedure to achieve optimal power allocation for DC-OFDM. For each modulation method, we quantify the received electrical SNR required at a given bit rate on a given channel, considering an ensemble of 170 indoor wireless channels. When using the same symbol rate for all modulation methods, *M*-PAM with MMSE-DFE has better performance than any OFDM format over a range of spectral efficiencies, with the advantage of (*M*-PAM) increasing at high spectral efficiency. ACO-OFDM and PAM-DMT have practically identical performance at any spectral efficiency. They are the best OFDM formats at low spectral efficiency, whereas DC-OFDM is best at high spectral efficiency. When ACO-OFDM or PAM-DMT are allowed to use twice the symbol rate of *M*-PAM, these OFDM formats have better performance than *M*-PAM. When channel state information is unavailable at the transmitter, however, *M*-PAM significantly outperforms all OFDM formats. When using the same symbol rate for all modulation methods, *M*-PAM requires approximately three times more computational complexity per processor than all OFDM formats and 63% faster analog-to-digital converters, assuming oversampling ratios of 1.23 and 2 for ACO-OFDM and *M*-PAM, respectively. When OFDM uses twice the symbol rate of *M*-PAM, OFDM requires 23% faster analog-to-digital converters than *M*-PAM but OFDM requires approximately 40% less computational complexity than *M*-PAM per processor.**

***Index Terms*—Optical wireless, infrared wireless, visible light communications, communications system performance, multicarrier optical systems, orthogonal frequency-division multiplexing, power allocation, intensity modulation with direct detection, PAM-DMT, ACO-OFDM, OOK, OFDM, MMSE equalizers.**

I. Introduction

INDOOR optical wireless transmission has been studied extensively in recent decades [1]–[4]. The visible and infrared spectral regions offer virtually unlimited bandwidth that is unregulated worldwide. Light in the infrared or visible range penetrates through glass, but not through walls or other opaque barriers, so that optical wireless transmissions are confined to the room in which they originate. Furthermore, in a visible or infrared wireless link employing intensity modulation with direct detection (IM/DD), the short carrier wavelength and large-area photodetector lead to efficient spatial diversity that prevents fading. Nevertheless, the existence of multiple paths between the transmitter and receiver causes multipath distortion, particularly in links using non-directional transmitters and receivers, or in links relying upon non-line-of-sight propagation [1],[2]. This multipath distortion can lead to intersymbol interference (ISI) at high bit rates.

Multicarrier modulation has been proposed to combat ISI in optical wireless links, since the symbol period of each subcarrier can be made long compared to the delay spread caused by multipath distortion [5]. Multicarrier modulation is usually implemented by orthogonal frequency-division multiplexing (OFDM) [3],[6],[7]. The main drawback of multicarrier modulation in systems using intensity modulation (IM) is the high DC bias required to make the multicarrier waveform nonnegative. There have been several approaches for reducing the DC bias in IM OFDM systems. The first technique uses hard-clipping on the negative signal peaks in order to reduce the DC bias required. This method is called DC-clipped OFDM (DC-OFDM) [3],[6]. Another technique clips the entire negative excursion of the waveform. Impairment from clipping noise is avoided by appropriate choice of the data-bearing subcarrier frequencies [7]. This technique is called asymmetrically clipped optical OFDM (ACO-OFDM) [7]. A third technique also clips the entire negative excursion, but modulates only the imaginary parts of the subcarriers such that the clipping noise becomes orthogonal to the desired signal. This technique is called PAM-modulated discrete multitone (PAM-DMT) [8].

There have been several studies comparing the performance of different OFDM techniques (e.g., [7]) but these comparisons have been made for ideal additive white Gaussian noise (AWGN) channels. To our knowledge, previous studies have not compared the OFDM methods to conventional baseband methods, such as on-off keying (OOK) or unipolar pulse-amplitude modulation (PAM), nor have they considered the dispersive nature of optical wireless channels. Furthermore, in previous work, the powers of the subcarriers and the DC bias for DC-OFDM were not jointly optimized according to the channel frequency response in order to obtain the lowest required optical power. We present an iterative procedure for

Paper approved by A. Bononi, the Editor for Optical Transmission and Networks of the IEEE Communications Society. Manuscript received October 21, 2010; revised July 9, 2011.

This work was supported by the Portuguese Foundation for Science and Technology scholarship SFRH/BD/22547/2005, and by a Stanford Graduate Fellowship.

D. J. F. Barros and J. M. Kahn are with the E. L. Ginzton Laboratory, Department of Electrical Engineering, Stanford University, Stanford, CA 94305-9515 USA (e-mail: djbarros@stanford.edu; jmk@ee.stanford.edu).

S. K. Wilson is with the Department of Electrical Engineering, Santa Clara University, Santa Clara, CA, USA (e-mail: skwilson@scu.edu).

Digital Object Identifier 10.1109/TCOMM.2011.112311.100538

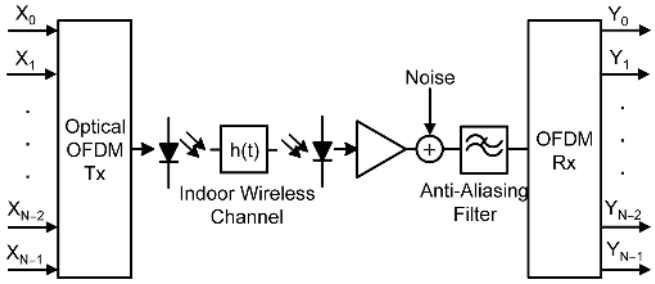

Fig. 1. System model for indoor optical wireless with direct-detection OFDM.

DC-OFDM based on known bit-loading algorithms with a new modification, the bias ratio, in order to obtain the optimum power allocation.

The optimum detection technique for unipolar PAM in the presence of ISI is maximum-likelihood sequence detection (MLSD), but its computational complexity increases exponentially with the channel memory. ISI in optical wireless links is well-approximated as linear in the instantaneous power [2], and for typical wireless links, PAM with minimum mean-square error decision-feedback equalization (MMSE-DFE) achieves nearly the same performance as MLSD and requires far less computational complexity. Hence, we compare the performance of the three aforementioned OFDM techniques using optimized power allocations to the performance of PAM with MMSE-DFE at different spectral efficiencies.

This paper is organized as follows. We present our system and indoor optical wireless models in Section II. In Section III, we review the different OFDM formats. In Section IV, we compare the receiver electrical SNR required to transmit at several bit rates for the different OFDM formats and for unipolar *M*-PAM with MMSE-DFE equalization at different spectral efficiencies. Furthermore, we compare the receiver electrical SNR required for the different modulation formats when there is no channel state information (CSI) available at the transmitter. We also compare the computational complexity required for OFDM and *M*-PAM at different bit rates. We present conclusions in Section V.

II. System Model and Performance Measures

A. Overall System Model

The OFDM system model is shown in Fig. 1.

An OFDM modulator encodes transmitted symbols onto an electrical OFDM waveform and modulates this onto the instantaneous power of an optical carrier at infrared or visible frequencies. The modulator can generate one of DC-OFDM, ACO-OFDM or PAM-DMT. Details of modulators for particular OFDM schemes are described in Section III. After propagating through the indoor wireless link, the optical signal intensity is detected and the electrical photocurrent is low-pass filtered. Since we are trying to minimize the optical power required to transmit at given bit rate R_b, we assume the receiver operates in a regime where signal shot noise is negligible, and the dominant noise is the shot noise from detected background light or thermal noise from the preamplifier following the photodetector. After low-pass filtering, the electrical OFDM signal is demodulated and equalized with a single-tap equalizer on each subcarrier to compensate for channel distortion [9].

B. Optical Wireless Channel

Multipath propagation in an indoor optical wireless channel [10],[11] can be described by an impulse response $h(t)$ or by the corresponding baseband frequency response $H(f) = \int_{-\infty}^{\infty} h(t) e^{-j2\pi ft} dt$. Including noise, the baseband channel model is [2]:

$$y(t) = R \cdot x(t) * h(t) + n(t), \tag{1}$$

where $y(t)$ is the detected photocurrent, $x(t)$ is the transmitted intensity waveform, R is the photodetector responsivity, and $n(t)$ represents ambient light shot noise and thermal noise. Optical wireless channels differ from electrical or radio frequency channels because the channel input $x(t)$ represents instantaneous optical power. Hence, the channel input is nonnegative $(x(t) \geq 0)$ and the average transmitted optical power P_t is given by

$$P_t = \lim_{T \to \infty} \frac{1}{2T} \int_{-T}^{T} x(t)\, dt, \tag{2}$$

rather than the usual time-average of $|x(t)|^2$, which is appropriate when $x(t)$ represents amplitude. The average received optical power can be written as

$$P = H(0) P_t, \tag{3}$$

where $H(0)$ is the DC gain of the channel, i.e., $H(0) = \int_{-\infty}^{\infty} h(t)\, dt$.

We use the methodology developed by Barry et al [10] to simulate the impulse responses of indoor optical wireless channels, taking account of multiple bounces. A similar model can be found in [12]. The algorithm in [10] partitions a room into many elementary reflectors and sums up the impulse response contributions from k^{th}-order bounces, $h^{(k)}(t)$, $k = 0, 1, 2, \ldots$. More recently, Carruthers developed an iterative version of the multi-bounce impulse response algorithm which greatly reduces the computational time required to accurately model optical wireless channels [13]. In this study, we use a toolbox developed by Carruthers to implement the algorithm in [13].

We place the transmitter and receiver in a room with dimensions 8 m $\times$ 6 m $\times$ 3 m (length, width, height). Room surfaces are discretized with a spatial resolution of 0.2 m, and are assumed to have diffuse reflectivities as in configuration A in [10]. All the source and receiver parameters are the same as in configuration A in [10]. We assume the transmitter has a Lambertian radiation pattern, with intensity per unit solid angle proportional to the cosine of the angle with respect to the transmitter normal [10]. We also assume that the receiver area is equal to 1 cm^2 and it only detects light whose angle of incidence is less than 90° with respect to the receiver normal [10]. According to [13], considering three to five bounces in calculating the impulse response should be sufficient to accurately model most indoor environments with typical reflectivities and geometries. Hence, we consider five bounces.

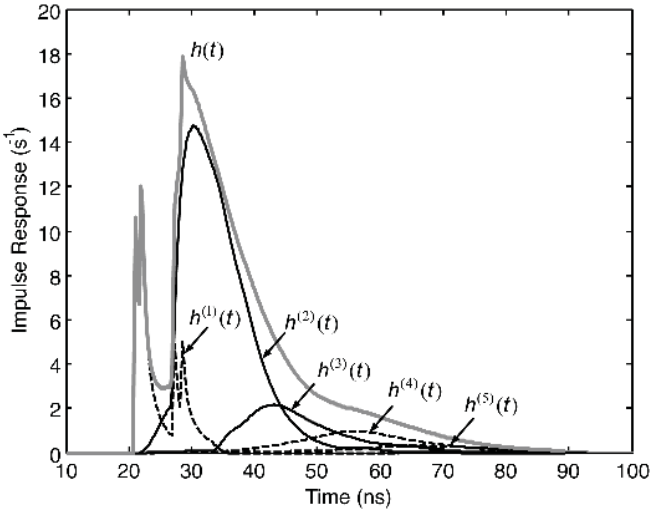

Fig. 2. Impulse response of an exemplary non-directional, non-LOS (diffuse) channel. This channel has no LOS component $h^{(0)}(t)$. The contributions of the first five reflections, $h^{(1)}(t), \ldots, h^{(5)}(t)$, are shown.

We generate 170 different channels by placing the transmitter in different locations within the room. In all channel realizations, the receiver is placed in the middle of the room 1 m above the floor and pointed upward. Our channel ensemble includes line-of-sight (LOS) configurations (transmitter placed at the ceiling and pointed down) and diffuse configurations (transmitter placed 1 m above the floor and pointed up). In order to simulate shadowing by a person or object next to the receiver, we block the LOS path (i.e., $h^{(0)}(t)$) of some of the impulse responses. Fig. 2 shows the impulse response for an exemplary diffuse channel from our set.

III. Analysis of Direct-Detection OFDM Schemes

A. DC-Clipped OFDM

The main disadvantage of using OFDM with intensity modulation is the DC bias required to make an OFDM signal nonnegative. Since OFDM signals have a high peak-to-average amplitude ratio, the required DC bias can be high. A simple approach to reducing the DC bias γ is to perform hard-clipping on the negative signal peaks [3]. This technique is usually called DC-OFDM. A DC-OFDM transmitter is shown in Fig. 3. In Fig. 3, the transmitted symbols are modulated such that the time-domain waveform is real. This is achieved by enforcing Hermitian symmetry in the symbols input to the inverse discrete Fourier transform (IDFT). We note that the zero (DC) subcarrier is not modulated, and is equal to the DC bias. After digital-to-analog (D/A) conversion, the electrical OFDM signal is hard-clipped such that the waveform becomes nonnegative, and then the signal is intensity modulated onto the optical carrier.

For a large number of subcarriers, we can model the electrical OFDM signal $x(t)$ as a Gaussian random variable with mean equal to the DC bias γ and variance equal to the electrical power $\sigma^2 = E\left[|x(t)|^2\right]$. After hard-clipping at zero, we obtain only the positive side of the Gaussian distribution. We show in Appendix A that the average optical power of

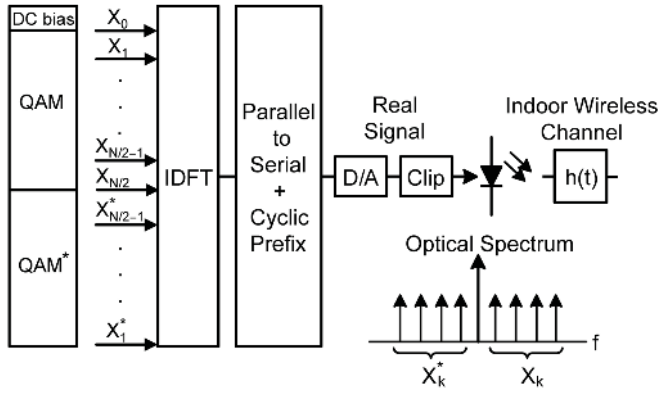

Fig. 3. Block diagram of a DC-OFDM transmitter.

DC-OFDM is given by

$$P_{DC-OFDM} = E\left[x_{clip}(t)\right] = \frac{\sigma}{\sqrt{2\pi}} e^{-\frac{\gamma^2}{2\sigma^2}} + \gamma\left(1 - Q\left(\frac{\gamma}{\sigma}\right)\right), \tag{4}$$

where Q is the Gaussian Q function [14]. We note that if the DC bias is chosen such that there is no clipping, then the optical power is equal to the DC bias γ, as expected.

In computing the optimized subcarrier power allocation for DC-OFDM, we cannot use the water-filling equations [14] directly, since the clipping noise on each subcarrier depends on the power of all the subcarriers. Thus, we perform the power allocation iteratively. We use an approach similar to that in [15]. For a given power allocation, the SNR measured at each subcarrier is used to compute an updated water-filling solution. We repeat this process until the power allocation no longer changes. In addition to optimizing the power and bit allocation at each subcarrier, we need to optimize the optical power $P_{DC-OFDM}$. In order to minimize the optical power, we use a DC bias level γ proportional to the square-root of the electrical power, as in [15]:

$$\gamma = K_b \cdot \sigma, \tag{5}$$

where K_b is a proportionality constant, which we refer to as the *bias ratio*. This ensures that the water-filling solution minimizes the required optical power. Fig. 4 shows the flow chart for power minimization of DC-OFDM using the bias ratio. For example, if, at iteration k, the electrical power is high after subcarrier power allocation, the DC bias will also be high (since it is proportional to the square-root of electrical power), and the optical power will be high. We note that a high DC bias reduces clipping noise and therefore increases the electrical SNR on each subcarrier. At the next iteration $k+1$, the water-filling algorithm will reduce the electrical power to lower the electrical SNR, thereby reducing the DC bias and the optical power. On the other hand, if, at iteration k, the DC bias is low, the clipping noise will be high, and the electrical SNR on each subcarrier will be low. At the next iteration $k+1$, the water-filling algorithm will add electrical power to increase the electrical SNR, and consequently the DC bias and optical power will increase.

For a given value of the bias ratio K_b, we repeat this process until the power allocation and DC bias γ no longer change. The minimum required optical SNR is obtained by performing

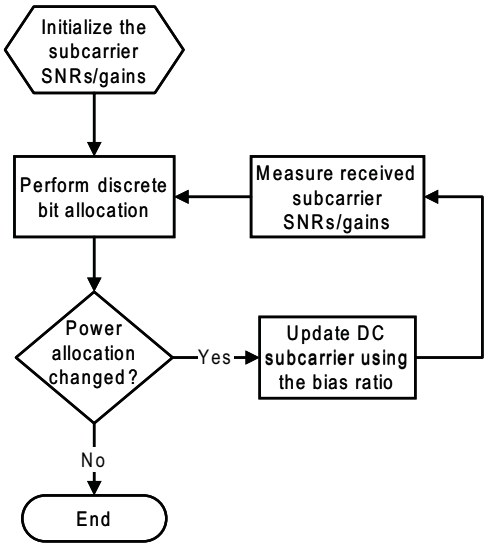

Fig. 4. Flow chart of DC-OFDM optimization using the bias ratio.

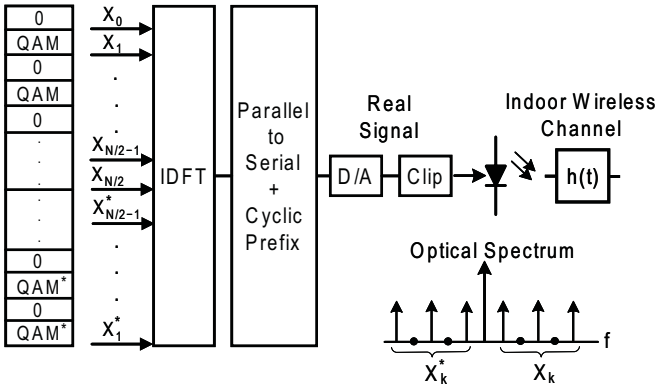

Fig. 5. Block diagram of an ACO-OFDM transmitter.

an exhaustive search over the value of the bias ratio K_b, as shown for the example in [15].

B. Asymmetrically Clipped Optical OFDM

Armstrong and Lowery proposed setting the DC bias γ to zero, and showed that impairment from clipping noise is avoided by encoding information symbols on only the odd subcarriers [7]. This technique is called ACO-OFDM. Fig. 5 shows a block diagram of an ACO-OFDM transmitter.

As in DC-OFDM, the OFDM subcarriers are assumed to have Hermitian symmetry, to ensure a real time-domain waveform. Because only the odd subcarriers are used to transmit data, for a given choice of signal constellation, ACO-OFDM has only half the spectral efficiency of DC-OFDM. After D/A conversion, the electrical OFDM signal is hard-clipped at zero and intensity modulated onto an optical carrier.

For a large number of subcarriers, we can again model the electrical OFDM signal $x(t)$ as a Gaussian random variable, but for ACO-OFDM, the electrical signal has zero mean. Armstrong and Lowery showed that for ACO-OFDM, the average and variance of the electrical waveform are $\sigma/\sqrt{2\pi}$ and $\sigma^2/2$, respectively [16]. Hence, the average optical power

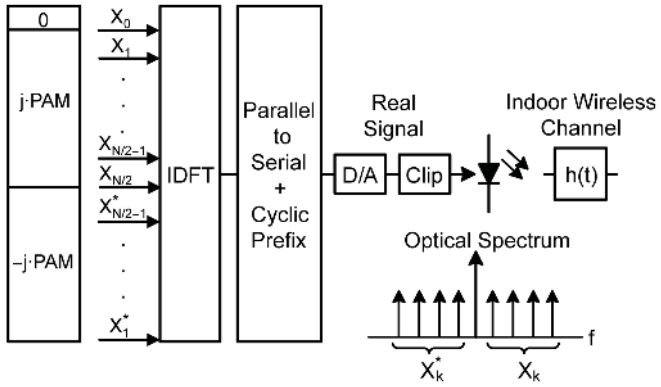

Fig. 6. Block diagram of a PAM-DMT transmitter.

for ACO-OFDM is

$$P_{ACO-OFDM} = \frac{\sigma}{\sqrt{2\pi}}. \tag{6}$$

We observe in Eq. (6) that the average optical power is proportional to the square-root of the electrical power.

C. PAM-Modulated Discrete Multitone

Similar to ACO-OFDM, PAM-DMT [8] clips the entire negative excursion of the electrical waveform to minimize average optical power. Lee and Koonen [8] showed that if data is modulated using PAM only on the imaginary components of the subcarriers, clipping noise does not affect system performance since that noise is real valued, and is thus orthogonal to the modulation. Fig. 6 shows a block diagram of a PAM-DMT transmitter.

As in DC-OFDM and ACO-OFDM, the subcarriers for PAM-DMT have Hermitian symmetry, so that the time-domain waveform is real. Contrary to ACO-OFDM, in PAM-DMT, all of the subcarriers are used, but the modulation is restricted to just one dimension. Hence, PAM-DMT has the same spectral efficiency as ACO-OFDM. After D/A conversion, the electrical OFDM signal is hard-clipped at zero and intensity modulated onto an optical carrier.

Using an analysis similar to that for ACO-OFDM, Lee and Koonen showed that the average transmitted optical power for PAM-DMT is given by [8]

$$P_{PAM-DMT} = \frac{\sigma}{\sqrt{2\pi}}, \tag{7}$$

where σ is the square-root of the electrical power of the OFDM waveform.

IV. Comparison of Direct-Detection Modulation Formats

In the following analysis, we use the system model shown in Fig. 1 in Section II-A. We employ the wireless channel model discussed in Section II-B. We model the dominant noise as real baseband AWGN with zero mean and double-sided power spectral density $N_0/2$. We assume a photodetector quantum efficiency of 90%, which corresponds, for example, to a responsivity of $R = 0.6$ A/Hz at 850 nm. At the receiver, the anti-aliasing filter is a fifth-order Butterworth low-pass

TABLE I
SYSTEM PARAMETERS FOR THE VARIOUS MODULATION FORMATS FOR DIFFERENT BIT RATES AND SYMBOL RATES. N IS THE DFT SIZE, N_u IS THE NUMBER OF USED SUBCARRIERS, ν IS THE CYCLIC PREFIX, N_f IS THE NUMBER OF TAPS OF THE FEEDFORWARD FILTER, N_b IS THE NUMBER OF TAPS OF THE FEEDBACK FILTER AND B_e IS THE REQUIRED ELECTRICAL BANDWIDTH IN MHZ

Bit Rate (Mbit/s)	DC-OFDM		ACO-OFDM		PAM-DMT		OOK
	R_S	$2{\cdot}R_S$	R_S	$2{\cdot}R_S$	R_S	$2{\cdot}R_S$	R_S
50	$N=512$ $N_u=208$ $\nu=10$ $B_e=25$	$N=512$ $N_u=208$ $\nu=12$ $B_e=50$	$N=1024$ $N_u=208$ $\nu=10$ $B_e=25$	$N=1024$ $N_u=208$ $\nu=12$ $B_e=50$	$N=1024$ $N_u=416$ $\nu=10$ $B_e=25$	$N=1024$ $N_u=416$ $\nu=12$ $B_e=50$	$N_f=28$ $N_b=6$ $B_e=50$
100	$N=512$ $N_u=208$ $\nu=12$ $B_e=50$	$N=512$ $N_u=208$ $\nu=15$ $B_e=100$	$N=1024$ $N_u=208$ $\nu=12$ $B_e=50$	$N=1024$ $N_u=208$ $\nu=15$ $B_e=100$	$N=1024$ $N_u=416$ $\nu=12$ $B_e=50$	$N=1024$ $N_u=416$ $\nu=15$ $B_e=100$	$N_f=44$ $N_b=10$ $B_e=100$
300	$N=512$ $N_u=208$ $\nu=18$ $B_e=150$	$N=1024$ $N_u=416$ $\nu=26$ $B_e=300$	$N=1024$ $N_u=208$ $\nu=18$ $B_e=150$	$N=2048$ $N_u=416$ $\nu=26$ $B_e=300$	$N=1024$ $N_u=416$ $\nu=18$ $B_e=150$	$N=2048$ $N_u=832$ $\nu=26$ $B_e=300$	$N_f=98$ $N_b=28$ $B_e=300$

filter. For OFDM, we set the 3-dB cutoff frequency of the anti-aliasing filter equal to the first null of the OFDM spectrum [9]. For *M*-PAM, we set the 3-dB cutoff frequency to $0.8R_s$, where R_s is the symbol rate. We note that the anti-aliasing filter cannot cause noise enhancement for any of the modulation formats, since the noise is added before the anti-aliasing filter. In other words, the performance comparison between the modulation formats is independent of the anti-aliasing filter type, given an adequate receiver oversampling ratio and an adequate cyclic prefix length or number of equalizer taps.

We would like to minimize the oversampling ratios for OFDM and *M*-PAM in order to minimize the A/D sampling frequency while still obtaining optimal performance. In OFDM, oversampling is performed by inserting zero subcarriers, and hence, it is possible to employ arbitrary rational oversampling ratios. For OFDM, we find that an oversampling ratio $M_s = 64/52 \approx 1.23$ is sufficient to obtain optimal performance. For *M*-PAM, arbitrary rational oversampling ratios are possible, but require complex equalizer structures [17]. While good performance can be achieved at an oversampling ratio of 3/2, we choose an oversampling ratio of 2, since it achieves slightly better performance than 3/2 while minimizing equalizer complexity. Note that in this case, OOK requires an A/D sampling frequency 63% higher than OFDM.

Typical high-performance forward error-correction (FEC) codes for optical systems have a bit-error ratio (BER) thresholds of the order of $P_b = 10^{-3}$ [18]. In order for our system to be compatible with such FEC codes while providing a small margin, we compute the minimum required SNR to achieve $P_b = 10^{-4}$ for the different modulation formats.

On a bipolar channel with AWGN, the optimum power and bit allocations for an OFDM system are given by the water-filling solution [14]. While the optimal value for the number of bits for each subcarrier is an arbitrary nonnegative real number, in practice, the constellation size and FEC code rate need to be adjusted to obtain a rational number of bits. The optimal discrete bit allocation method on bipolar channels is known as the Levin-Campello algorithm [19]. In this algorithm, we first set the desired bit granularity β for each subcarrier, i.e., the bit allocation on each subcarrier is an integer multiple of β. In our study, we choose a granularity $\beta = 0.25$, since it is straightforward to design codes whose rates are multiples of 0.25 [20]. Furthermore, we observe that there is no significant performance difference between OFDM with discrete loading ($\beta = 0.25$) and with continuous loading.

In order to compare the average optical power requirements of different modulation techniques at a fixed bit rate, we define electrical SNR as [2]

$$SNR = \frac{R^2 P^2}{N_0 R_b} = \frac{R^2 H^2(0) P_t^2}{N_0 R_b}, \tag{8}$$

where R_b is the bit rate and N_0 is the (single-sided) noise power spectral density. The electrical SNR given by Eq. (8) is proportional to the square of the received optical signal power P, in contrast to conventional electrical systems, where it is proportional to the received electrical signal power. Hence, a 2-dB change in the electrical SNR (8) corresponds to a 1-dB change in average optical power.

A. OOK and OFDM Performance

In this section, we analyze the effect of delay spread on the required SNR for different modulation formats at a spectral efficiency of 1 bit/symbol. We present our results using the normalized delay spread D_T, which is the rms delay spread D divided by the information bit period $T_b (T_b = 1/R_b)$ [21]. The normalized delay spread D_T is known to be a useful measure of multipath-induced ISI to, at least when using OOK or pulse-position modulation (PPM) [11],[21].

We let R_s denote the symbol rate for unipolar *M*-PAM (for 2-PAM or OOK, $R_s = R_b$). We let R_s^{OFDM} denote the equivalent symbol rate for OFDM [9]. In order to perform a fair comparison at a given fixed bit rate R_b between unipolar *M*-PAM and OFDM, we initially set the two symbol rates to be equal: $R_s^{OFDM} = R_s$ [14].

Fig. 7 shows the electrical SNR required to achieve bit rates of 50, 100 and 300 Mbit/s for all channels using ACO-OFDM and OOK. In Fig. 7, the symbol rates are the same for both modulation schemes, i.e., $R_s^{OFDM} = R_s$, and they are chosen to be 50, 100 and 300 MHz, respectively. The receiver and transmitter electrical bandwidths are scaled accordingly to the symbol rate in use. For ACO-OFDM with a symbol rate of 300 MHz, the FFT size is $N = 1024$ and the number of used subcarriers is $N_u = 208$. We set the cyclic prefix equal to three times the rms delay spread (D) of the worst impulse response, corresponding to $\nu = 18$ samples measured at the OFDM

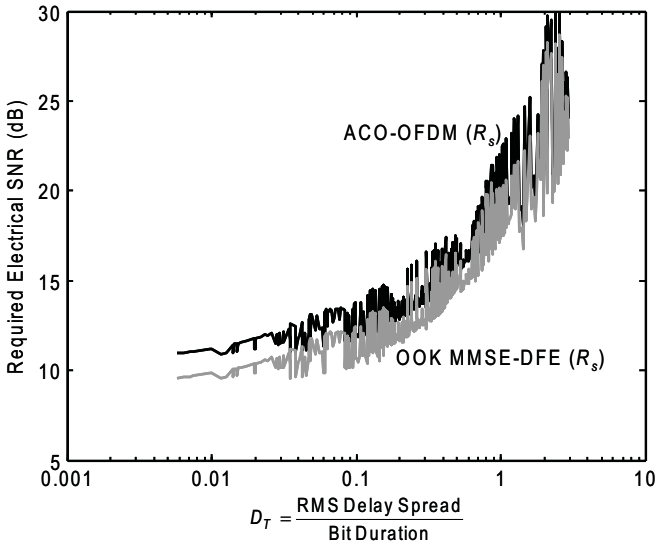

Fig. 7. Electrical SNR required to achieve $P_b = 10^{-4}$ vs. normalized delay spread D_T at bit rates of 50, 100 and 300 Mbit/s (spectral efficiency of 1 bit/symbol) for ACO-OFDM and OOK. The bit allocation granularity is $\beta = 0.25$ and the symbol rates for ACO-OFDM are the same as those for OOK, as indicated.

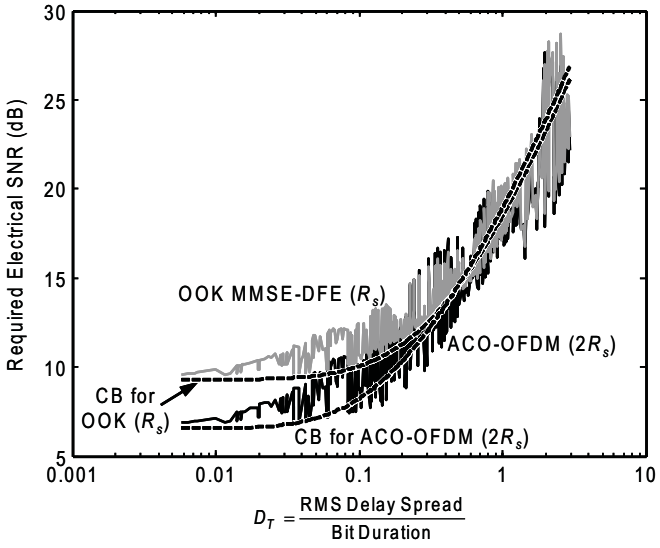

Fig. 8. Electrical SNR required to achieve $P_b = 10^{-4}$ vs. normalized delay spread D_T at bit rates of 50, 100 and 300 Mbit/s (spectral efficiency of 1 bit/symbol) for different modulations formats. The dashed lines correspond to the SNR requirement predicted using the ceiling-bounce (CB) model. The bit allocation granularity is $\beta = 0.25$ and the symbol rates for ACO-OFDM are twice those for OOK, as indicated.

symbol rate. For OOK, we use a fractionally spaced MMSE-DFE at an oversampling ratio of 2. We use the same number of taps for all wireless channels, which is chosen based on the worst channel: 98 taps for the feedforward filter and 28 taps for the feedback filter when the symbol rate is 300 MHz. The parameters for the various modulation formats and bit rates are listed in Table 1.

In Fig. 7, we notice that as the normalized delay spread increases, the available electrical bandwidth decreases and hence more power is required to maintain the bit rate. We also observe that ACO-OFDM requires a higher SNR than OOK for all channels in our set when both modulations use the same symbol rates to transmit the same bit rates. In this case, which corresponds to a spectral efficiency of 1 bit/symbol, the performance difference is about 1.3 dB. ACO-OFDM requires a higher SNR than OOK because it requires an average of 4 bits (16-QAM constellation) on the used subcarriers to compensate the information rate loss of setting half of the subcarriers to zero.

One option to improve the performance of OFDM is to use more electrical bandwidth in order to reduce the constellation size on each subcarrier. We define electrical bandwidth (B_e)[1] as the span from DC to the location of the first spectral null of the power spectral density (PSD) of the transmitted waveform $x(t)$ [2]. At a symbol rate R_s, M-PAM with rectangular non-return-to-zero (NRZ) pulses requires an electrical bandwidth of approximately $B_e^{PAM} \approx R_s$. On the other hand, OFDM at symbol rate R_s^{OFDM} only requires an electrical bandwidth of only $B_e^{OFDM} \approx R_s^{OFDM}/2$ [9], since it has a more confined spectrum. Hence, for the same symbol rate as M-PAM $(R_s^{OFDM} = R_s)$, OFDM requires about half the bandwidth of M-PAM with rectangular NRZ pulses. If we double the symbol rate for OFDM, both modulations schemes use approximately the same electrical bandwidth: $B_e^{OFDM} = B_e^{PAM} = R_s$. The electrical bandwidth required for all modulation formats is summarized in Table 1. However, we note that when OFDM uses twice the symbol rate of M-PAM, OFDM uses twice the electrical bandwidth it would normally require to transmit the same bit rate as M-PAM. We also note that when the OFDM symbol rate is doubled, OFDM requires an analog-to-digital (A/D) converter sampling frequency of $M_s R_s^{OFDM} = M_s \cdot 2R_s$, which is 23% higher than the sampling frequency required for M-PAM using an oversampling ratio of 2. We also want to point out that the usable electrical bandwidth becomes eventually limited by the channel multipath distortion. Hence, for channels with high delay spreads, there is very little benefit in increasing the transmitter and receiver electrical bandwidths.

Having the previous considerations in mind, we study the trade-off between electrical bandwidth and SNR performance for OFDM in Figs. 8 and 9. Fig. 8 shows the receiver electrical SNR required to achieve the bit rates of 50, 100 and 300 Mbit/s when ACO-OFDM uses twice the symbol rate of OOK, i.e., $R_s^{OFDM} = 2R_s$. The symbol rates for OOK are 50, 100 and 300 MHz, respectively and the symbol rates for ACO-OFDM are 100, 200 and 600 MHz, respectively. The receiver and transmitter electrical bandwidths are scaled according to the symbol rate in use.

In Fig. 8, we observe that ACO-OFDM using twice the symbol rate of OOK requires the lowest SNR to achieve a $P_b = 10^{-4}$ for all channels at the bit rates of 50, 100 and 300 Mbit/s. For low delay spreads $(D_T < 0.1)$, corresponding to LOS channels, ACO-OFDM significantly outperforms OOK. For high delay spreads, however, OOK with MMSE-DFE performs very close to ACO-OFDM. We again note that when

[1]We note that the electrical bandwidth of a modulation technique has little influence on the optical bandwidth B_o occupied by an IM signal when using typical light sources (e.g., a light emitting diodes or multimode laser diodes) [2], since the optical bandwidth B_o is dominated by the source linewidth. For example, a 1-nm linewidth corresponds to 469 GHz, assuming a wavelength of 800 nm.

OFDM uses twice the symbol rate of OOK, OFDM uses twice the bandwidth it would normally require to transmit the same bit rate as OOK. Even with this advantage, for a given bit rate, ACO-OFDM achieves approximately the same performance as OOK for high delay spreads, as shown in Fig. 8. ACO-OFDM performs better for low delay spreads because it can use more bandwidth and transmit lower constellation sizes on each subcarrier. For high delay spreads, the wireless channel becomes more bandwidth-constrained, and there is very little gain by using more bandwidth for ACO-OFDM.

In Fig. 8, we also show the SNR requirements for OOK and ACO-OFDM estimated using the *ceiling-bounce (CB) model* [21]. Carruthers and Kahn [21] found a simple functional approximation of the impulse response that exhibits approximately the same relationship between ISI penalty and normalized delay spread D_T as a wide ensemble of experimentally measured channels, at least for OOK and PPM [21]. We observe that the CB model provides a reasonable is estimate of the SNR requirement. We note that in computing Fig. 8 for OOK with MMSE-DFE, we have assumed correct decisions at the input of the feedback filter.

In order to make a fair comparison with ACO-OFDM, the number of used subcarriers in DC-OFDM should be the same as for ACO-OFDM. For PAM-DMT, since only one dimension is used to transmit data, the number of used subcarriers should be twice that for ACO-OFDM. In computing the optimized subcarrier power allocation for DC-OFDM, we use an iteratively water-filling solution with the bias ratio K_b, as defined in Eq. (5), performing an exhaustive search over the value of K_b, as in [15]. We have plotted the SNR requirements for DC-OFDM and PAM-DMT separately in Fig. 9, in order to make Fig. 8 more legible.

Fig. 9 shows the cumulative distribution function (CDF) of the required electrical SNR, which is defined as:

$$CDF(SNR) = \text{Prob}\,(x \leq SNR) \tag{9}$$

where SNR takes all possible values for the required SNR for a given modulation format. We assume that all 170 channels realizations occur with equal probability. The CDF corresponds to the fraction of channels on which the target P_b is reached at a given SNR. For example, Fig. 9 shows that if the transmitter has CSI and the electrical SNR is at least 30 dB, the target $P_b \leq 10^{-4}$ is met for all the channels when using ACO-OFDM (or PAM-DMT) at any of the three bit rates, 50, 100 or 300 Mbit/s.

We observe in Fig. 9, as in Fig. 8, that ACO-OFDM using twice the symbol rate of OOK requires the lowest SNR to achieve a $P_b = 10^{-4}$. On the other hand, if ACO-OFDM uses the same symbol rate as OOK, OOK is more power efficient. Furthermore, we verify that there is no significant performance difference between ACO-OFDM and PAM-DMT. This is expected, since it was proven in [22] that ACO-OFDM and PAM-DMT achieve very similar performance on low-pass channels. Finally, we observe that DC-OFDM requires the highest SNR because of the optical power used in the DC bias to reduce clipping noise.

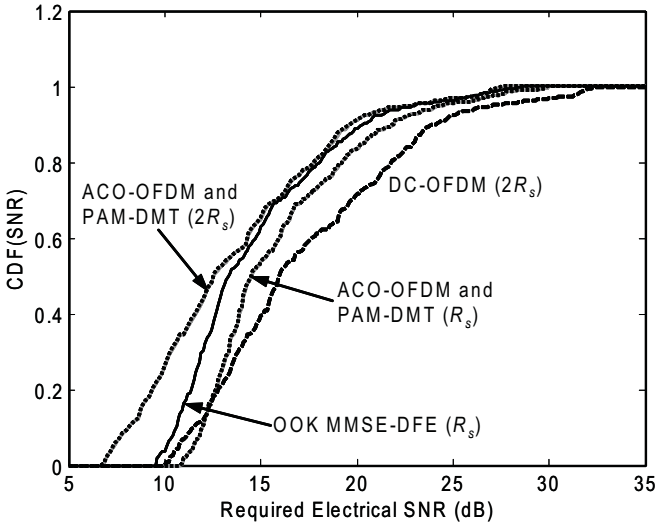

Fig. 9. Cumulative distribution function (CDF) of the electrical SNR required to achieve $P_b = 10^{-4}$ at bit rates of 50, 100 and 300 Mbit/s (spectral efficiency of 1 bit/symbol) for different modulation formats. The symbol rates for OFDM are the same as or twice those for OOK, as indicated.

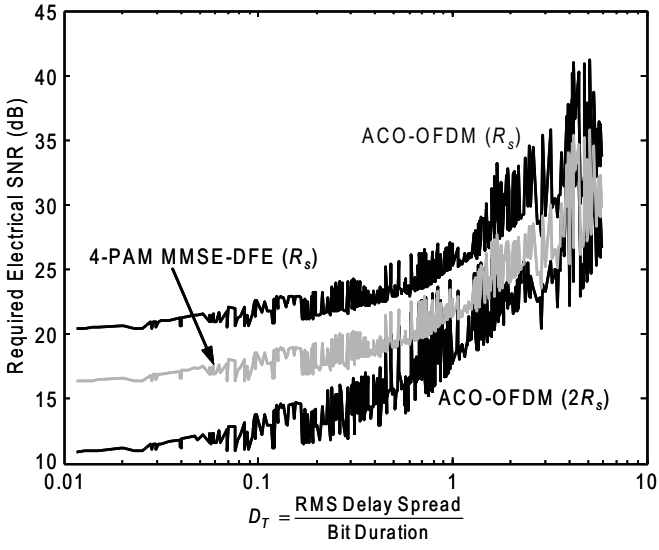

Fig. 10. Electrical SNR required to achieve $P_b = 10^{-4}$ vs. normalized delay spread D_T at bit rates of 100, 200 and 600 Mbit/s (spectral efficiency of 2 bit/symbol) for different modulations formats. The bit allocation granularity is $\beta = 0.25$ and the symbol rates for ACO-OFDM are the same as or twice those for 4-PAM, as indicated.

B. Unipolar 4-PAM and OFDM Performance

In this section, we compare the performance of the different modulation formats at higher spectral efficiencies to check if there are any significant differences from the previous section. Figs. 10 and 11 show the electrical SNR required to achieve bit rates of 100, 200 and 600 Mbit/s for different modulation formats at a spectral efficiency of 2 bit/symbol. The symbol rates for unipolar 4-PAM are 50, 100 and 300 MHz, respectively. The receiver and transmitter electrical bandwidths are scaled according to the symbol rate in use.

In Figs. 10 and 11, we observe that ACO-OFDM and PAM-DMT using twice the symbol rate of 4-PAM again requires the lowest SNR for all channels. In Fig. 11, we observe again that PAM-DMT has the same performance as ACO-

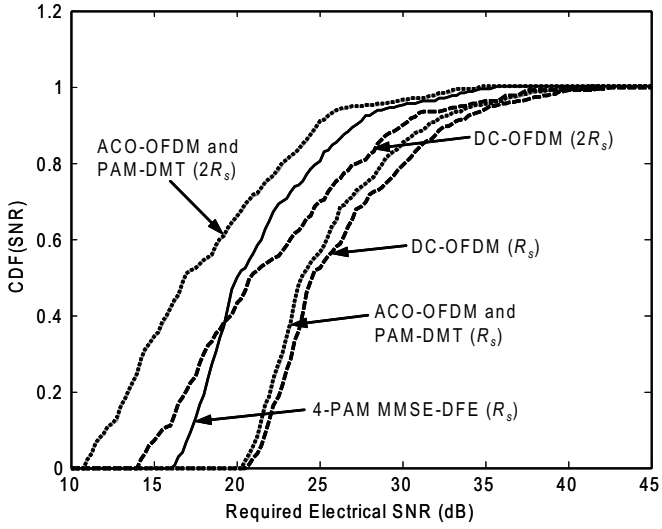

Fig. 11. Cumulative distribution function (CDF) of the electrical SNR required to achieve $P_b = 10^{-4}$ at bit rates of 100, 200 and 600 Mbit/s (spectral efficiency of 2 bit/symbol) for different modulation formats. The symbol rates for OFDM are the same as or twice those for 4-PAM, as indicated.

OFDM for any symbol rate. Since both modulations have the same performance, we choose ACO-OFDM as our basis of comparison for the remainder of the paper. The performance improvement for ACO-OFDM (and PAM-DMT) in Figs. 10 and 11 requires doubling the bandwidth and increasing the sampling frequency, which becomes 23% higher than the sampling frequency required for 4-PAM with an oversampling ratio of 2. Comparing Figs. 9 and 11, we see that the performance difference between ACO-OFDM with twice the symbol rate and 4-PAM increases with the spectral efficiency. We also observe in Fig. 11 that DC-OFDM with twice the symbol rate performs close to 4-PAM.

When all the modulations use equal symbol rates, 4-PAM requires the lowest SNR of all the modulation formats, and the difference in SNR between ACO-OFDM (or PAM-DMT) and unipolar 4-PAM is about 4 dB. We conclude that increasing the spectral efficiency from 1 bit/symbol (Fig. 9) to 2 bit/symbol (Fig. 11) increases differences in SNR requirements between ACO-OFDM and (M-PAM) from 1 dB to 4 dB. This is to be expected, since increasing the spectral efficiency from 1 bit/symbol to 2 bit/symbol for ACO-OFDM requires doubling the average transmitted number of bits on each subcarrier from 4 bits (16-QAM) to 8 bits (256-QAM). For higher spectral efficiencies, ACO-OFDM require constellations that are increasingly large and therefore (M-PAM) has increasingly better performance than ACO-OFDM with equal symbol rates.

Finally, we also note in Fig. 11 that DC-OFDM performs very close to ACO-OFDM (or PAM-DMT) when the OFDM symbol rate is the same as that for 4-PAM and the spectral efficiency is 2 bit/symbol. This is because the clipping noise penalty in DC-OFDM becomes less significant when compared to the additional SNR required to transmit higher constellation sizes in each ACO-OFDM subcarrier.

Although DC-OFDM uses twice as many subcarriers as ACO-OFDM (or PAM-DMT) to transmit data, the clipping noise and DC bias limit the power efficiency of DC-OFDM for a spectral efficiency of 1 bit/symbol, as shown in Fig. 9. However, as spectral efficiency increases, the clipping noise penalty in DC-OFDM becomes less significant when compared to the additional SNR required to transmit higher constellation sizes in each ACO-OFDM subcarrier, and eventually DC-OFDM performs better than ACO-OFDM.

C. Outage Probability

It is also useful to analyze the receiver performance when the transmitter does not have CSI. This happens, for example, in a broadcast configuration where the transmitter sends the same information to several receivers or when there is no return path from the receiver (i.e., uplink). When CSI is unavailable at the transmitter, some data-bearing subcarriers might be lost due to multipath distortion. Hence, we use coding across the subcarriers such that the information can be recovered from the good subcarriers. We choose a shortened Reed-Solomon (RS) code with $(n, k) = (127, 107)$ over GF(2^8) with hard decision decoding (HDD) for simplicity.[2] In order for the comparison between OFDM and OOK to be fair, OOK also employs this code.

We consider a channel realization to be in outage if $P_b > 10^{-4}$ for a desired bit rate. We define outage probability P_{outage} as the fraction of channels with $P_b > 10^{-4}$ over the entire ensemble of channels realizations. In practice, a system might not be expected to work on the most severe channel realizations (e.g., shadowed channels), but in our study we include all channels as a worst-case scenario.

We assume a desired bit rate of 300 Mbit/s. For OOK, we increase the symbol rate from 300 MHz to 356 MHz to compensate for coding overhead. For OFDM, we use ACO-OFDM with twice the data symbol rate of OOK, i.e., 600 MHz. We compensate for the information loss due to coding by increasing the constellation size on each subcarrier. The same performance could be achieved with PAM-DMT.

We assume that the channel changes slowly enough such that many OFDM blocks are affected by a channel realization. In this scenario, there is no benefit to using time diversity (e.g., interleaving) in the bit allocation on the subcarriers. We also assume that the transmitter has knowledge of the *mean channel*, which has a frequency response defined by:

$$H_{mean}(f) = \frac{1}{N_{\text{realiz}}} \sum_{k=1}^{N_{\text{realiz}}} H_k(f), \tag{10}$$

which is an average over all 170 channel realizations. For ACO-OFDM, we consider three different bit allocation schemes: *mean channel loading*, where the transmitter does integer bit loading using the frequency response of the mean channel; *ceiling-bounce loading*, where the transmitter performs integer bit allocation on a ceiling-bounce channel having

[2]In an optimized implementation, this code (used to recover subcarriers lost due to multipath distortion) might be integrated with the outer FEC code (used to combat additive noise) into a single concatenated coding scheme. Likewise, more powerful coding schemes (such as turbo or low-density parity-check codes) could be used to recover the lost subcarriers. Given the simple nature of indoor optical wireless channels, we would expect our conclusions to remain valid even if more optimized coding schemes were employed.

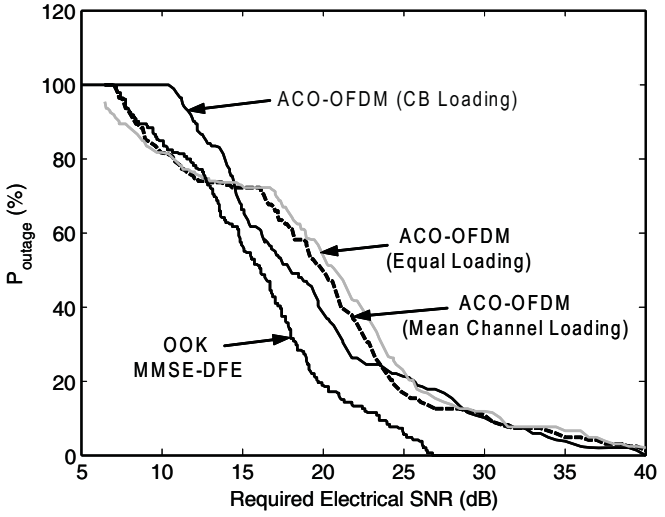

Fig. 12. Outage probability for OOK and ACO-OFDM with coding and various bit allocations averaged over all channels. All modulation formats use the code RS(127,107) over GF(2^8). The information bit rate is 300 Mbit/s (spectral efficiency of 1 bit/symbol) and the symbol rates for OOK and OFDM are 356 MHz and 600 MHz, respectively. The bit allocation granularity is $\beta = 1$, i.e., integer bit allocation.

the same rms delay spread D as the mean channel,[3] and *equal loading*, where all the subcarriers carry the same number of bits. After having performed the bit allocation, we sweep the transmitter power and observe which channel realizations are in outage, i.e., have $P_b > 10^{-4}$.

Since each RS block in OFDM has a different uncoded P_b, we simulate RS decoding with error counting in order to obtain the correct P_b after RS decoding. For OOK, we use a binomial expansion to obtain P_b after RS decoding, since each bit has the same uncoded P_b.

Fig. 12 shows the outage probability for coded ACO-OFDM and coded OOK with MMSE-DFE for a desired bit rate of 300 Mbit/s.

We observe that OOK has a significantly lower outage probability than OFDM for the same SNR. In other words, when the transmitter does not have CSI, OOK with MMSE-DFE performs better than ACO-OFDM with twice the symbol rate, in contrast to Figs. 9 and 11. Results for 50 and 100 Mbit/s are qualitatively similar to those for 300 Mbit/s, particularly at low outage probabilities. These results are not shown in Fig. 12 to maximize legibility. At low outage probabilities ($P_{outage} < 10\%$), CB loading performs slightly better than the other loading schemes. For outage probabilities between 25% and 70%, CB loading is significantly better than the other schemes. For high outage probabilities, equal loading performs the best. Finally, we observe that over a wide range of outage probabilities, mean channel loading generally outperforms equal loading. We note that when the outage probability is high, the system can only operate on channels having low delay spreads, which are generally those without shadowing. In practice, a user could improve performance by moving his receiver to avoid shadowing.

[3]For the purpose of computing the rms delay spread D of the mean channel, the impulse response of the mean channel is computed as the inverse Fourier transform of $H_{mean}(f)$.

D. Computational Complexity

For OFDM, the IDFT and DFT operations are performed efficiently using a fast Fourier transform (FFT) algorithm. An FFT of size N requires approximately $4 \cdot N \cdot \log_2(N)$ real operations (multiplications plus additions) [23]. Thus, the number of real operations required per second for the transmitter is $4 \cdot N \cdot \log_2(N)/T_{OFDM}$, where T_{OFDM} is the OFDM symbol period, which is given in [9]. For the OFDM receiver, we need to take into account the complex single-tap equalizer on each used subcarrier. Assuming that complex multiplications are implemented with the usual 4 real multiplications and 2 real additions [23], the number of real operations required per second for the receiver is $(4 \cdot N \cdot \log_2(N) + 6 \cdot N_u)\, T_{OFDM}$, where N_u is the number of used subcarriers. The overall complexity order in real operations per bit for OFDM is

$$\begin{aligned} O_{OFDM}^{Tx}(N) &= 4N\log_2(N)T_b/T_{OFDM} \\ &= \frac{4N\log_2(N)M_sT_bR_s^{OFDM}}{N+\nu\cdot M_s} \\ O_{OFDM}^{Rx}(N) &= [4N\log_2(N)+6N_u]\,T_b/T_{OFDM} \\ &= \frac{[4N\log_2(N)+6N_u]\,M_sT_bR_s^{OFDM}}{N+\nu\cdot M_s} \end{aligned} \quad (11)$$

For *M*-PAM, the complexity of directly implementing the convolution operation for the DFE is $2(N_f+N_b)/T_s$ complex operations (multiplications plus additions) per second, where N_f is the number of taps of the feedforward filter, N_b is the number of taps of the feedback filter and T_s is the symbol period ($T_s = 1/R_s = T_b \cdot \log_2 M$). The equalizer computes an output once per symbol interval. The overall complexity order in real operations per bit for *M*-PAM in a direct implementation is

$$\begin{aligned} O_{PAM}^{D}(N) &= [4(N_f+N_b)+4(N_f+N_b)]\,T_b/T_s \\ &= 8(N_f+N_b)\,T_b/T_s \\ &= 8(N_f+N_b)/\log_2 M \end{aligned} \quad (12)$$

For a large number of taps, linear equalization is more efficiently implemented using an FFT-based block processing such as overlap-add or overlap-save [14]. Suppose a block length of L is chosen. An FFT-based implementation has a complexity of $(N_{taps}+L-1)\cdot(4\times 2\cdot\log_2(N_{taps}+L-1)+6)$ real operations per block L for an equalizer with N_{taps} taps. For a given N_{taps}, there exists an optimum block length L that minimizes the number of operations required. We assumed that the equalizer taps come from a lookup table since indoor optical wireless channels typically change slowly and therefore the same equalizer taps can be used for many symbols. The overall complexity order in real operations per bit for *M*-PAM with a DFE in a FFT implementation is

$$\begin{aligned} O_{PAM}^{FFT}(N) &= \frac{(N_f+L_f-1)\cdot(8\cdot\log_2(N_f+L_f-1)+6)}{B_f\log_2 M} \\ &\quad + \frac{(N_b+L_b-1)\cdot(8\cdot\log_2(N_b+L_b-1)+6)}{B_b\log_2 M} \end{aligned} \quad (13)$$

where L_f and L_b are the block sizes for the feedforward and feedback filters, respectively.

TABLE II
COMPUTATIONAL COMPLEXITY IN REAL OPERATIONS PER BIT FOR THE VARIOUS MODULATION FORMATS

Bit Rate (Mbit/s)		50	100	300
ACO-OFDM (R_S)	Tx	48.5	48.5	48.1
	Rx	50.0	50.0	49.6
ACO-OFDM ($2{\cdot}R_S$)	Tx	97.0	96.7	106.5
	Rx	100.0	99.6	109.4
PAM-DMT (R_S)	Tx	48.5	48.5	48.1
	Rx	51.5	51.5	51.1
PAM-DMT ($2{\cdot}R_S$)	Tx	97.0	96.7	106.5
	Rx	102.9	102.6	112.4
DC-OFDM (R_S)	Tx	43.0	43.0	42.4
	Rx	45.9	45.9	45.3
DC-OFDM ($2{\cdot}R_S$)	Tx	86.1	85.4	95.3
	Rx	91.9	91.2	101.1
OOK (R_S)	L_f	101	213	415
	L_b	59	119	229
	FFT	137.2	150.8	174.5
	Direct	272	432	1008

Using the parameters in Table 1, we compute the number of operations required per bit for OOK and OFDM in Table 2. For OOK, we calculate the complexity of direct implementation and FFT based implementation using optimized block sizes L_f and L_b subject to having a FFT size that is an integer power of two. In Table 2, we observe that an OFDM system with twice the symbol rate of OOK requires two digital signal processors (DSPs) with approximately 40% less computational complexity than the single DSP required for OOK. On the other hand, an OFDM system requires an A/D and D/A while OOK requires only one A/D. We also note that DC-OFDM has the lowest computational complexity among OFDM formats, since it uses smaller FFT sizes than ACO-OFDM or PAM-DMT.

V. CONCLUSIONS

On indoor optical wireless channels, we have evaluated the performance of three different IM/DD OFDM formats, DC-OFDM, ACO-OFDM and PAM-DMT, and have compared them to unipolar *M*-PAM with MMSE-DFE. We have shown how to minimize the average optical power required for DC-OFDM to achieve a specified error probability by iteratively adjusting the subcarrier power allocation and the bias ratio. When using the same symbol rate for all modulation methods, we have found that unipolar *M*-PAM with MMSE-DFE has better optical power efficiency than all OFDM formats over a range of spectral efficiencies. Furthermore, we have found that as spectral efficiency increases, the performance advantage of *M*-PAM increases, since the OFDM formats require increasingly large signal constellations. We have also found that ACO-OFDM and PAM-DMT have virtually identical performance at any spectral efficiency. They are the best OFDM formats at low spectral efficiency, but as spectral efficiency increases, DC-OFDM performs closer to ACO-OFDM, since the clipping noise penalty for DC-OFDM becomes less significant than the penalty for the larger constellations required for ACO-OFDM. When ACO-OFDM or PAM-DMT are allowed to use twice the symbol rate of *M*-PAM, these OFDM formats have better performance than *M*-PAM. However, at a spectral efficiency of 1 bit/symbol, OOK with MMSE-DFE has performance similar to ACO-OFDM or PAM-DMT for high delay spreads. When CSI is unavailable at the transmitter, *M*-PAM significantly outperforms all OFDM formats even when they use twice the symbol rate of *M*-PAM. When using the same symbol rate for all modulation methods, *M*-PAM requires approximately three times more computational complexity per DSP than all OFDM formats and 63% faster A/D converters. When OFDM uses twice the symbol rate of *M*-PAM, OFDM requires 23% faster A/D converters than (*M*-PAM) but OFDM requires 40% less computational complexity than *M*-PAM per DSP.

APPENDIX

Derivation of the average of the clipped OFDM waveform is crucial to optimization of the average optical power. For a large number of subcarriers, we can model the electrical OFDM signal $x(t)$ as a Gaussian random variable with mean equal to the DC bias γ and variance equal to the electrical power $\sigma^2 = E\left[|x(t)|^2\right]$. After hard-clipping at zero, we obtain only the positive side of the Gaussian distribution. The average optical power is equal to the average of the clipped waveform and can be written as

$$P_{opt} = E\left[x_{clip}(t)\right] = \int_0^{+\infty} x \cdot N\left(\gamma, \sigma^2\right) dx, \qquad \text{(A-1)}$$

where $N\left(\gamma, \sigma^2\right)$ is the Gaussian pdf with mean γ and variance σ^2. Doing a variable change, $z = x - \gamma$, we obtain

$$\begin{aligned} E\left[x_{clip}(t)\right] &= \int_{-\gamma}^{+\infty} (z+\gamma) \cdot N\left(0, \sigma^2\right) dz \\ &= \gamma \int_{-\gamma}^{+\infty} N\left(0, \sigma^2\right) dz + \int_{-\gamma}^{+\infty} z \cdot N\left(0, \sigma^2\right) dz, \\ &= \gamma\left(1 - Q\left(\frac{\gamma}{\sigma}\right)\right) + \frac{\sigma}{\sqrt{2\pi}} e^{-\frac{\gamma^2}{2\sigma^2}} \qquad \text{(A-2)} \end{aligned}$$

where Q is the Gaussian Q function [12]. For ACO-OFDM, the DC bias is $\gamma = 0$ and Eq. (A2) simplifies to Eq. (6).

REFERENCES

[1] F. R. Gfeller and U. Bapst, "Wireless in-house data communication via diffuse infrared radiation," *Proc. IEEE*, vol. 67, no. 11, pp. 1474–1486, Nov. 1979.

[2] J. M. Kahn and J. R. Barry, "Wireless infrared communications," *Proc. IEEE*, vol. 85, no. 2, pp. 265–298, 1997.

[3] O. Gonzalez, R. Perez-Jimenez, S. Rodriguez, J. Rabadan, and A. Ayala, "Adaptive OFDM system for communications over the indoor wireless optical channel," *IEE Proc. – Optoelectronics*, vol. 153, no. 4, pp. 139–144, 2006.

[4] H. Joshi, R. J. Green, and M. S. Leeson, "Multiple sub-carrier optical wireless systems," in *Proc. ICTON 2008*, vol. 4, pp. 184–188.

[5] J. B. Carruthers and J. M. Kahn, "Multiple-subcarrier modulation for non-directed wireless infrared communication," *IEEE J. Sel. Areas Commun.*, vol. 14, no. 3, pp. 538–546, Apr. 1996.

[6] S. K. Wilson and J. Armstrong, "Transmitter and receiver methods for improving asymmetrically-clipped optical OFDM," *IEEE Trans. Wireless Commun.*, vol. 8, no. 9, pp. 4561–4567, 2009.
[7] J. Armstrong and B. J. C. Schmidt, "Comparison of asymmetrically clipped optical OFDM and DC-biased optical OFDM in AWGN," *IEEE Commun. Lett.*, vol. 12, no. 5, pp. 343–345, 2008.
[8] S. C. J. Lee, S. Randel, F. Breyer, and A. M. J. Koonen, "PAM-DMT for intensity-modulated and direct-detection optical communication systems," *IEEE Photon. Technol. Lett.*, vol. 21, no. 23, pp. 1749–1751, 2009.
[9] D. J. F. Barros and J. M. Kahn, "Optimized dispersion compensation using orthogonal frequency-division multiplexing," *J. Lightwave Technol.*, vol. 26, no. 16, pp. 2889–2898, 2008.
[10] J. R. Barry, J. M. Kahn, W. J. Krause, E. A. Lee, and D. G. Messerschmitt, "Simulation of multipath impulse response for wireless optical channels," *IEEE J. Sel. Areas Commun.*, vol. 11, no. 3, pp. 367–379, 1993.
[11] J. M. Kahn, W. J. Krause, and J. B. Carruthers, "Experimental characterization of non-directed indoor infrared channels," *IEEE Trans. Commun.*, vol. 43, no. 234, pp. 1613–1623, Apr. 1995.
[12] J. Grubor, O. C. Gaete Jamett, J. W. Walewski, S. Randel, and K.-D. Langer, "High-speed wireless indoor communication via visible light," *ITG FACHBERICHT*, 2007.
[13] J. B. Carruthers and P. Kannan, "Iterative site-based modeling for wireless infrared channels," *IEEE Trans. Antennas Propag.*, vol. 50, no. 5, pp. 759–765, 2002.
[14] J. G. Proakis, *Digital Communications*, 4th edition. McGraw-Hill, 2001.
[15] D. J. F. Barros and J. M. Kahn, "Comparison of orthogonal frequency-division multiplexing and on-off keying in amplified direct-detection single-mode fiber systems," *J. Lightwave Technol.*, vol. 28, no. 12, pp. 1811–1820, 2010.
[16] J. Armstrong and A. J. Lowery, "Power efficient optical OFDM," *Electron. Lett.*, vol. 42, no. 6, pp. 370–372, 2006.
[17] E. Ip and J. M. Kahn, "Digital equalization of chromatic dispersion and polarization mode dispersion," *J. Lightwave Technol.*, vol. 25, no. 8, pp. 2033–2043, 2007.
[18] E. Forestieri, *Optical Communication Theory and Techniques*. Springer, 2005.
[19] J. Campello, "Optimal discrete bit loading for multicarrier modulation systems," in *Proc. IEEE Symp. Info. Theory 1998*.
[20] T. J. Richardson and R. L. Urbanke, *Modern Coding Theory*. Cambridge University Press, 2008.
[21] J. B. Carruthers and J. M. Kahn, "Modeling of nondirected wireless iInfrared channels," *IEEE Trans. Commun.*, vol. 45, no. 10, pp. 1260–1268, 1997.
[22] D. J. F. Barros and J. M. Kahn, "Comparison of orthogonal frequency-division multiplexing and on-off keying in direct-detection multimode fiber links," to be published.
[23] S. G. Johnson and M. Frigo, "A modified split-radix FFT with fewer arithmetic operations," *IEEE Trans. Signal Process.*, vol. 55, no. 1, pp. 111–119, Jan. 2007.

Daniel J. F. Barros received the "Licenciatura" degree (with honors) in electrical and electronics engineering from the University of Porto, Portugal, in 2004, and the M.S. and Ph.D. degrees in electrical engineering from Stanford University, Stanford, CA, in 2007 and 2011, respectively. His research interests include optical fiber communications, wireless communications, digital signal processing, and RF circuits.

Sarah Kate Wilson (M'87-SM'99) received her A.B. from Bryn Mawr College with honors in mathematics in 1979 and her Ph.D. from Stanford University in electrical engineering in 1994. She has worked in both industry and academia and has been a visiting professor at Lulea University of Technology, the Royal Institute of Technology in Stockholm, and Stanford University. She is currently on the faculty of Santa Clara University. She has served as an associate editor for the IEEE TRANSACTIONS ON WIRELESS COMMUNICATIONS, IEEE COMMUNICATIONS LETTERS, and the IEEE TRANSACTIONS ON COMMUNICATIONS. She has served as an associate editor for the IEEE TRANSACTIONS ON WIRELESS COMMUNICATIONS, IEEE COMMUNICATIONS LETTERS, the IEEE TRANSACTIONS ON COMMUNICATIONS, and the *Journal of Communications and Networks*. She is currently the Editor-in-Chief of IEEE COMMUNICATIONS LETTERS and a member-at-large of the IEEE Communications Society Board of Governors for the term 2009–2012.

Joseph M. Kahn (M'90-SM'98-F'00) received the A.B., M.A., and Ph.D. degrees in physics from U.C. Berkeley in 1981, 1983, and 1986, respectively. From 1987–1990, he was at AT&T Bell Laboratories, Crawford Hill Laboratory, in Holmdel, NJ. He demonstrated multi-Gb/s coherent optical fiber transmission systems, setting world records for receiver sensitivity. From 1990–2003, he was on the faculty of the Department of Electrical Engineering and Computer Sciences at U.C. Berkeley, performing research on optical and wireless communications. Since 2003, he has been a Professor of electrical engineering at Stanford University, where he heads the Optical Communications Group. His current research interests include: rate-adaptive and spectrally efficient modulation and coding methods, coherent detection and associated digital signal processing algorithms, digital compensation of fiber nonlinearity, high-speed transmission in multimode fiber, and free-space systems. Professor Kahn received the National Science Foundation Presidential Young Investigator Award in 1991. He is a Fellow of the IEEE. From 1993–2000, he served as a Technical Editor of *IEEE Personal Communications Magazine*. Since 2009, he has been an Associate Editor of the IEEE/OSA JOURNAL OF OPTICAL COMMUNICATIONS AND NETWORKING. In 2000, he helped found StrataLight Communications (now Opnext Subsystems), where he served as Chief Scientist from 2000–2003.